A&A manuscript no.
(will be inserted by hand later)

Your thesaurus codes are:
08(08.07.1,08.09.2,08.16.2,13.09.6)

ASTRONOMY AND ASTROPHYSICS

A very cold disc of dust around the G0V star HD 207129 ⋆

M. Jourdain de Muizon[1,2], R.J. Laureijs[3], C. Dominik[4], H.J. Habing[4], L. Metcalfe[3], R. Siebenmorgen[3], M.F. Kessler[3], P. Bouchet[5], A. Salama[3], K. Leech[3], N. Trams[3], and A. Heske[3]

[1] DESPA, Observatoire de Paris, 92190 Meudon, France
[2] LAEFF–INTA, ESA Vilspa, PO Box 50727, 28080 Madrid, Spain. e-mail: muizon@laeff.esa.es
[3] ISO Data Center, Astrophysics Division, Space Science Department of ESA, Villafranca del Castillo, P.O. Box 50727, 28080 Madrid, Spain
[4] Leiden Observatory, P.O. Box 9513, 2300 RA Leiden, The Netherlands
[5] Cerro Tololo Inter-American Observatory, NOAO, Casilla 603, La Serena, Chile 1353

Received: ; accepted:

Abstract. We present ISO observations made between 2.5 and 180 μm of the nearby G0V dwarf HD 207129 taken as part of a large survey of nearby main-sequence stars in search of debris discs. HD 207129 emits radiation in excess of the photospheric flux density between at least 60 and 180 μm. The infrared excess is explained by a disc of cold dust particles (25 to 50 K) and, to account for the absence of a significant 25 μm excess, the disc must have a central hole of several 100 AU radius. We discuss various models and show how the disc will evolve in time under the influence of radiation pressure and Poynting-Robertson drift. The presence of the large hole suggests that HD 207129 has at least one planet.

Key words: Stars: Planetary systems – Stars: general – Stars: individual: HD 207129 – Infrared: stars

1. Introduction

During photometric calibration measurements of the IRAS satellite, Aumann et al. (1984) discovered by chance that α Lyr (alias Vega) had far-infrared ($\lambda > 10 \mu m$) emission in excess of the photospheric flux. Later on, a similar excess was found in several other main-sequence stars such as α PsA (alias Fomalhaut), β Pic and ϵ Eri (see Backman & Paresce 1993, for a review, and references therein). This excess was attributed to a circumstellar disc of solid particles similar to, but with much more material than, the disc that produces the Zodiacal Light. This interpretation was supported by an I-band coronographic picture of β Pic which shows a disc seen edge-on (Smith & Terrile 1984). The disc is interpreted as a left-over from the time when the star formed. which implies that the formation of a flat disc of material around the Sun has not been a unique event. To avoid confusion we call these systems "extrasolar systems" which implies that the discs may consist of dust, gas and planets. The discovery by Aumann et al. was the first evidence for an "extrasolar" system around a main-sequence star and is therefore of major astronomical interest (Backman & Paresce 1993; Jayawardhana et al. 1998).

This serendipitous discovery by Aumann et al. (1984) opened new lines of research that led to other discoveries: (i) massive discs around stars shortly before they arrive on the main sequence, e.g. TTau variables (Sargent & Beckwith 1987) and Herbig AeBe stars (Malfait et al. 1998; Mannings & Sargent 1997); (ii) planets around main-sequence stars (Mayor & Queloz 1995); (iii) discs around red giants (Plets et al. 1997; Plets & Vynckier 1999); (iv) the first circumstellar disc around a massive star (Stecklum et al. 1998). These observations suggest that discs may be present throughout the life of a star.

We undertook a photometric survey of main-sequence stars of spectral type A to K in the mid- and far-infrared wavelength range using the "Infrared Space Observatory", ISO (Kessler et al. 1996). Compared to IRAS, ISO offered two improvements: it reached lower sensitivity values (35 mJy noise, 1σ, at 100 μm) and it also measured wavelengths between 100 and 200 μm. This new survey has been presented in a preliminary version in Habing et al. (1996) and will appear more completely in Habing et al. (1999). We present in this paper one star from our sample, the G-dwarf HD 207129, a star already reported by Walker & Wolstencroft (1988) as having an excess at 60 μm, although based only on an IRAS flux of 0.25 Jy at 60 μm. The star caught our attention because we detected excess emission at 150 and 180 μm but only marginal excess at 25 μm. This suggested that the disc was significantly colder than those of Vega and β Pic. We therefore decided to obtain complementary ISO measurements.

The star HD 207129, also known as HR 8323 and as # 838 in the Catalogue of Nearby Stars by Gliese (1969), is of spectral type G0V and has a V-magnitude of 6.18. Its distance as measured by HIPPARCOS is 15.6 pc (ESA 1997; Perryman et al. 1997). From the strength of the Ca II chromospheric K emission line the star appears to have an age comparable to

Send offprint requests to: M. Jourdain de Muizon

⋆ Based on observations with ISO, an ESA project with instruments funded by ESA Member States (especially the PI countries: France, Germany, The Netherlands and the United Kingdom) with the participation of ISAS and NASA.

Table 1. Summary of observations, detailed descriptions of the observation modes are given in the text

filter	λ μm	aperture $''$/pixel	mode	date
PHT-SS	2.5–5	24×24	staring on/off	22/05/97
PHT-SL	6–12	24×24	staring on/off	22/05/97
P_3p6	3.6	23	staring on/off	22/05/97
CAM-LW2	14.3	3×3	coronographic	22/05/97
CAM-CVF	7–14	6×6	single pointing	22/05/97
P_7p7	7.7	23	staring on/off	22/05/97
P_12p8	12.8	52	staring on/off	22/05/97
P_20	20	52	staring on/off	22/05/97
P_25	25	52	staring on/off	22/05/97
P_25	25	52	chopped	31/03/96
C_60	60	46×46	chopped	31/03/96
C_90	90	46×46	chopped	31/03/96
C_135	150	92×92	minimap	27/10/96
C_135	150	92×92	chopped	31/03/96
C_160	170	92×92	minimap	27/10/96
C_180	180	92×92	chopped	31/03/96

the Sun (Pasquini 1992; Henry et al. 1996; Lachaume et al. 1999). Although the star has been observed on many occasions and by a variety of instruments there is no evidence for spectral peculiarities (apart from its IR excess) nor for one or more companions.

In Section 2, we describe the observations and in Section 3 the data reduction applied. In Section 4 and 5, we present and discuss respectively a simple and a more complex model for the cold disc observed, and we present conclusions in Section 6.

2. ISO Observations

The observations with the ISOPHOT instrument (Lemke et al. 1996) comprise of (spectro-)photometry at several far-infrared wavelengths to determine the spectral energy distribution of the infrared excess. Since the excess was expected to be weak (less than a few 100 mJy) we added photometry at the shorter wavelengths between 2.5 and 20 μm to assess the contribution of the stellar photosphere to the infrared flux. A summary of the observations is given in Table 1. All ISOPHOT observations except those with PHT-SS and SL include one or more calibration reference measurements of the fine calibration sources (FCSs) which is a tunable grey body mounted inside ISOPHOT. The FCSs have been calibrated against astronomical standards (Schulz et al. 1999).

The ISOPHOT observations were made in several filters and in different observing modes to enhance the reliability of the photometry. Initially the observations were performed by chopping the beam between the source and one ("rectangular chop") or two ("triangular chop") background reference positions using the chopper mirror inside the PHT instrument. We used triangular chop with $90''$ throw at 25, $150''$ throw at 60 and 90 μm and rectangular chop with $180''$ throw at 150 and 180 μm.

At a later stage we decided to observe in "minimap" mode at 150 and 170 μm (Table 1) in order to minimize uncertainties due to cirrus confusion which cannot be quantified unless full resolution mapping is performed. In the minimap mode a 3×3 points raster is obtained for each filter with $46''$ steps in both directions aligned with the C200 detector array orientation. This mode gives photometric results more reliable than the rectangular chop mode observations due to (1) a better determination of the source's background zero level and (2) the fact that the detector pixels are successively centred on the source providing a 4-fold redundancy.

The photometry in the 3.6–25 μm range using the P detectors comprise of staring observations first on a background position and subsequently on the source position. This way we ensured that the detector illumination increases as a function of time which minimizes transient behaviour of the detector responsivity. In addition we performed a chopped measurement at at 25 μm.

Observations with ISOCAM (Cesarsky et al. 1996) were obtained to map a possible spatial extent in the 15 μm region. This was done by performing coronographic CAM imaging in the LW3 band (12–18 μm), which has a reference wavelength of 14.3 μm. Because of the relatively strong intensity of the photospheric emission, the stellar light was blocked by selecting the small Fabry-mirror in combination with a $3''$ pixel field of view (PFOV) lens, thus causing the light at the edges of the array to be suppressed. By positioning the star on the outer edge of the CAM array, only the light from a possible extended emission could be seen by the array, any light coming from the star being cut off. This measurement was repeated on an adjacent edge, and for a number of positions of the source along the edge, to ensure a favourable alignment of any disc with respect to the array, and to ensure good rejection of any stray-light effects. At the distance of HD 207129, a disc of 500 AU radius would have an angular size of $33''$ which, for the observing configuration used, would have corresponded to several CAM pixels. This observation could only be done using a non-standard observing mode by means of the ISO calibration uplink system. Finally, a CAM–CVF spectrum was also obtained (details are given in Table 1).

3. Data Processing

The CAM–CVF scan on HD 207129 has been calibrated using standard techniques as described in the ISOCAM Data User's manual or IDUM (Siebenmorgen et al. 1998). After subtraction of the calibration dark, a residual dark pattern in the individual exposures could still be discerned. To remove this pattern a second order dark correction was applied. The IAS transient correction model (Abergel et al. 1996) was used to correct for detector transients. The integrated fluxes have been corrected for the part of the point spread function outside the integration area. Standard flat fields and the standard conversion from CAM instrumental units to Jy have been used.

For each CVF frame the background level was estimated from the mean brightness value of all neighbouring background

pixels. The background pixels were defined by masking the source emission. Multi-aperture photometry was simulated on each image.

CAM coronographic images for several positions of the star off the edge of the Fabry mirror were processed according to standard processing steps described in the CAM IDUM (Siebenmorgen et al. 1998) and using the ISOCAM Interactive Analysis software (Ott et al. 1997). Identical images obtained contiguously around the nearby reference star HD 210302 were subtracted from the target star images. The CAM instrument was specially configured to avoid any wheel movements between the target and reference star measurements. Having established that there was no apparent straylight contamination of the images, they were shifted and coadded to make a coronographic raster image of an L-shaped field surrounding the star, sufficient to overlap any disc whatever it's position angle. No structure was detected above the noise in the data. Simulated edge-on discs were inserted into the data with a range of surface brigthnesses in order to establish the faintest disc surface-brightness which would allow the disc to be seen above the noise, so setting an upper-limit for the flux of any undetected disc.

The ISOPHOT interactive analysis software (Gabriel et al. 1997a,b, PIA version 7.0,) has been used to process the ISOPHOT observations.

The staring measurements were processed according to standard ISOPHOT data reduction steps (Laureijs et al. 1998, see ISOPHOT IDUM). All measurements have been checked for responsivity transient variations. In case the signals stabilize during an integration, we removed the initial unstable parts of the measurement before taking the mean signal level. We have corrected the resulting 7.7 μm source signal for a non-linear response of the P1 detector. This was necessary because the source signals in 7.7 μm band are a factor 10 weaker than the signals in the 3.6 μm band for which the detector responsivity (via the FCS measurement) was determined. For such a large signal difference, responsivity non-linearities become important and cause systematic errors when using the same responsivity for both filters. The 12.8 μm measurements were calibrated with FCS measurements in the same filter and with comparable signal strength.

For the 20 and 25 μm staring observations, a drift model had to be applied to the FCS measurements to determine the final signal level. The 32 s duration of the FCS measurement with the P2 detector was not long enough for stabilization of the signals. We used the Fouks-Schubert correction model which is available in PIA. The corrected P2 responsivities are 20–30% lower than the uncorrected ones.

The chopped measurements at 60 and 90 μm with the C100 3×3 detector array were calibrated using the responsivity derived from the FCS measurement. No additional corrections for possible signal losses were applied. The source minus background signal of the centre pixel of the array (pixel 5) is used for the photometry. The same processing steps were applied to the chopped observations in the 150 and 180 μm bands with the C200 2×2 detector array. For these filters, the source minus background flux is determined by summing the flux densities measured in all 4 detector pixels.

The C200 minimaps were processed like normal staring observations. For each filter band the detector array was flat-fielded by assuming that each detector pixel accumulated the same total flux in the raster. Since there is one position in the raster where a detector pixel is centred on the source, we determined the source minus background flux for each detector pixel. The flux density of the source is the average over the 4 detector pixels. The scatter between the pixels is a measure of the uncertainty.

The flux densities are listed in Table 2. The point source flux densities have been obtained by dividing the fluxes per aperture or per pixel by the intensity fraction ($f_{\rm psf}$, see Table 2) of a point source centred on a given aperture, detector pixel, or detector array. For the staring measurements the uncertainties are obtained by propagating the statistical uncertainties in the detector signals. The uncertainties in the chopped observations were derived by taking 20% of the source flux if the statistical uncertainty derived from the signal distribution is less than 20%.

No attempt has been made to include possible systematic uncertainties in the absolute photometry calibration factors, relative filter calibration, and instrumental corrections. We estimate an absolute photometric accuracy for each filter of better than 20%. In the case of chopped observations the uncertainty could be higher, possibly as high as 50%.

The PHT–S observation on the star has been calibrated by using the spectral response function derived from a PHT–S measurement with same integration time of a calibration star with similar brightness. Assuming that detector responsivity transients are reproducible for identical flux steps, this method provides an empirical transient correction. The accuracy is determined by the reproducibility of the PHT–S detector responsivity which is known to be stable within a few percent as well as the accuracy of the predicted stellar flux of the calibration star.

4. Presentation of the Data and First Analysis

The CAM coronographic measurements provide an upper limit of 0.5 MJy/sr at 14.3 μm for the surface brightness of any disc out to a radius of 1 arcmin from the star with a spatial resolution of $6''$. The ISOPHOT photometric measurements are given in Table 2 and are plotted in Figure 4. The PHT–S and CAM–CVF spectra are plotted in Figure 3. The star appears to be a point source in the CAM–CVF observation with a $6''$ pixel size, therefore it is also a pointlike in the $24'' \times 24''$ PHOT–S aperture. Also plotted in Figures 3 and 4 are the IRAS Faint Source Catalogue fluxes (Moshir 1989) which are 897 mJy at 12 μm, 200 mJy at 25 μm, 301 mJy at 60 μm and an upper limit of 715 mJy at 100 μm. In Section 5, we have preferred to use the IRAS fluxes at 12 and 25 μm rather than the ISO chopped measurements.

The observed spectrum of HD 207129 (Figure 3 and Figure 4) is a power-law between 2.2 and 20 μm, thus defining the

Table 2. Flux densities resulting from ISO photometric measurements

filter	λ μm	Flux density mJy	Uncertainty mJy	Colour correction	$f_{\rm psf}$	IR excess mJy	Comment
P_3p6	3.6	6150	490	1.05	0.97		on-off, direct FCS
P_7p7	7.7	1217	146	1.02	0.93		on-off, applied non-lin corr.
P_12p8	12.8	494	35	1.02	0.90		on-off, direct FCS
P_20	20	336	50	1.01	0.76	110±50	on-off, Fouks drift model
P_25	25	257	39	1.28	0.70	90±40	on-off, Fouks drift model
P_25	25	366	103	1.28	0.70	90±40	chopped (default Resp)
C_60	60	291	58 (ch)	1.06	0.69	270±60	20% uncertainty (chopped)
C_90	90	283	57 (ch)	1.17	0.61	270±60	20% uncertainty (chopped)
C_135	150	285	47	1.10	0.66	320±40	minimap
C_135	150	588	118 (ch)	1.10	0.66	320±40	20% uncertainty (chopped)
C_160	170	352	28	1.20	0.64	350±30	minimap
C_180	180	408	82 (ch)	1.10	0.62	400±80	20% uncertainty (chopped)

Notes to Table 2: $f_{\rm psf}$ is the intensity fraction of a point source entering the aperture of PHT–P, or falling on one pixel of the C100 or C200 detectors. The uncertainties mentioned here do not account for systematic calibration errors. At 25 and 150 μm two types of measurement are available and, in these two cases, the value/uncertainty given for the "Infrared excess" is a weighted average/uncertainty of the two measurements. In column 7 (IR excess), the values obtained for the Infrared excess have been rounded according to the actual resulting uncertainty. In column 4 (Uncertainty), "(ch)" stands for "chopped measurement".

photosphere level. The extrapolation of this photospheric spectrum defines the zero-level from which any excess can be measured. In the 2 – 17 μm range, no dust feature, such as 9.7 μm silicate emission seen in some Vega-type stars (e.g. Sylvester et al. 1997), is detected above the noise level either in the PHT–S or the CAM–CVF spectra. In fact, there is no excess or dust feature detected at wavelengths shorter than 20 μm. The excess starts shortly beyond 25 μm. It is clearly strong already at 60 μm and extends at least as far as 200 μm, and most likely beyond.

Figure 2 shows the evidence of a 170 μm (broad band) detection, well above the cirrus level, thus proving that the excess goes at least as far as about 200 μm. If we are in the presence of a Vega-like disc, it must be very cold indeed.

The other possible causes of an excess, e.g. presence of a companion, of a planet, or alignment with a cirrus knot, can be rejected (see Dominik et al. 1998) and we interpret the excess in HD 207129 as the presence of a Vega-like disc around the star.

The excess that we detect in the far infrared starts around 25 μm and does not show any clear sign of fall-off as far as 200 μm, which is the long-wavelength limit of ISO. Interpreting this excess as due to a dust disc around the star, and with a grain emissivity law in λ^{-2}, our data points at 60, 150 and 170 μm indicate a dust temperature of 30 K.

The total luminosity of the disc is then estimated to be $1.4 \times 10^{-4}\,{\rm L}_{\odot}$. Following Hildebrand (1983), we obtain a total dust mass of ${\rm M}_d = 2.4 \times 10^{27} \times a_{\mu{\rm m}}$ grams, or $0.4 \times a_{\mu{\rm m}}\,{\rm M}_{\oplus}$, where $a_{\mu{\rm m}}$ is the average grain radius in μm.

Resolving the equations of energy balance of a dust grain of radius $a = 1\,\mu$m located in the disc around HD 207129 and using the absorption efficiencies for silicate grains given by Draine and Lee (1984), we find that the disc is at a distance from the star: $d = 1.85 \times 10^5 \times r_\star$, where $r_\star$ is the radius of the star, expressed in the same unit as d. The coefficient in this equation varies with the grain size, but for a stellar radius equal to the solar radius and for grain sizes ranging from 0.01 to 1 μm we obtain values of d between 550 and 850 AU. This distance can be compared to that of the Kuiper belt and the Oort cloud with respect to the Sun. The former starts at about 50 AU and its outer boundary may extend out to 10^3 AU (Weissman 1995). The so-called scattered Kuiper belt (objects on high excentricity orbits with perihelion near Neptune) goes out to a few hundred AU. The Oort cloud is at about 10^4 to 10^5 AU. Thus the estimated distance to the star of the HD 207129 disc makes it closer to a Kuiper belt type rather than an Oort cloud.

5. Modeling and Discussion

5.1. Stellar Photosphere

To obtain the essential stellar parameters we fitted a Kurucz atmosphere to the stellar photosphere of HD 207129. Using the Geneva colors as given in Burki *et al.* (1998), and the calibration of Geneva photometry (Rufener & Nicolet 1988) we derived the following parameters for the atmosphere: $T_{\rm eff} = 5933 \pm 26\ K$, $\log g = 4.66 \pm 0.14$, $[Z/H] = -0.08 \pm 0.09$. The resulting interpolated Kurucz model (Kurucz 1993) is consistent with the available visual magnitudes (see Figure 1). In the infrared, the model is a few percent lower than our spectral data points. This deviation is within the limitations of the model and we have used this fit to predict the photospheric flux at longer wavelengths (see Figure 3).

At wavelengths longer than 20 μm the star shows an infrared excess (Figure 4). By subtracting the flux given by the Kurucz model that best fits the photospheric flux from the total observed flux we obtain the fraction of the flux reemitted in the infrared: $L_{\rm IR} = 1.1 \times 10^{-4} L_*$, a typical value for "the

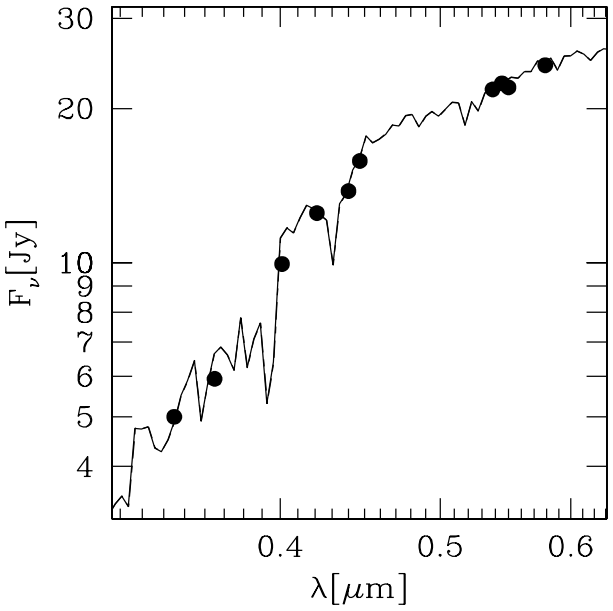

Fig. 1. The optical part of the Kurucz atmosphere fitted to the measured magnitudes of HD 207129. The big dots indicate magnitude measurements taken from the Geneva photometry catalogue (Burki *et al.* 1998, website)

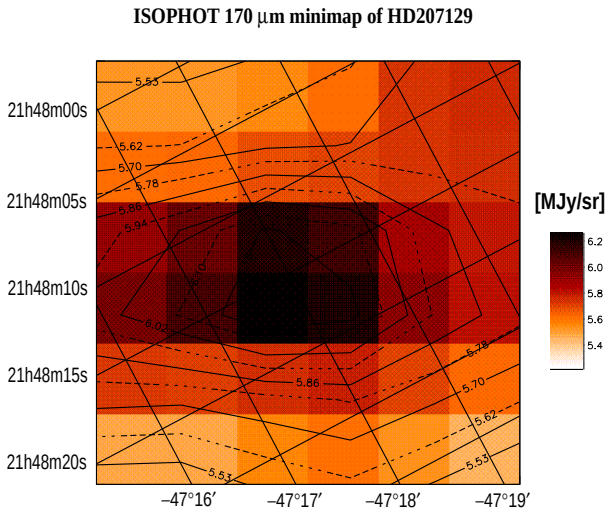

Fig. 2. ISOPHOT minimap of HD 207129 at 170 μm. Minimum flux at the edges of the map is about 5.5 MJy/sr, and at the centre we detect a flux of 6.2 MJy/sr.

Vega-phenomenon" around main-sequence stars (Backman & Paresce 1993).

The excesses above the predicted photosphere are listed in Table 2.

5.2. Disc model

In order to account for the far IR excess emission we have developed a disc model to explain the observations. Such a model is not unique in particular because only integrated photometric

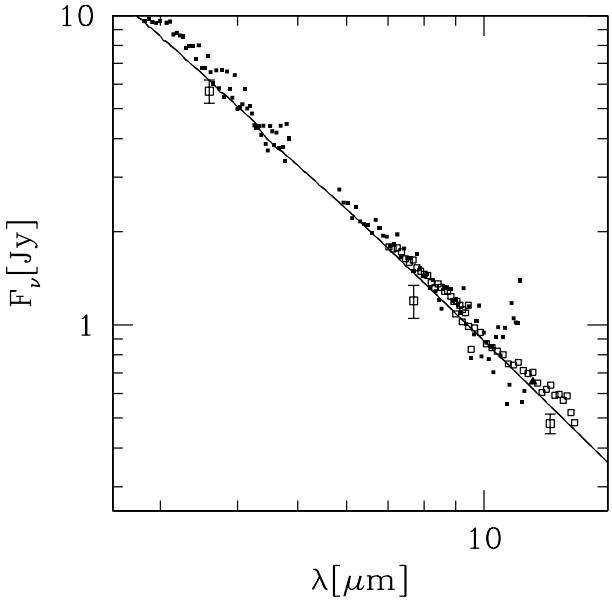

Fig. 3. The near and mid-IR region of the SED of HD 207129. The small squares indicate measurements from PHT–S (filled squares) and CAM–CVF (open squares) spectra. The larger spread in the points near 10 μm is due to increased noise at the fainter flux levels of PHT–S. The large square indicate photometry with ISOPHOT P. The triangle at 12 μm is taken from the IFSC.

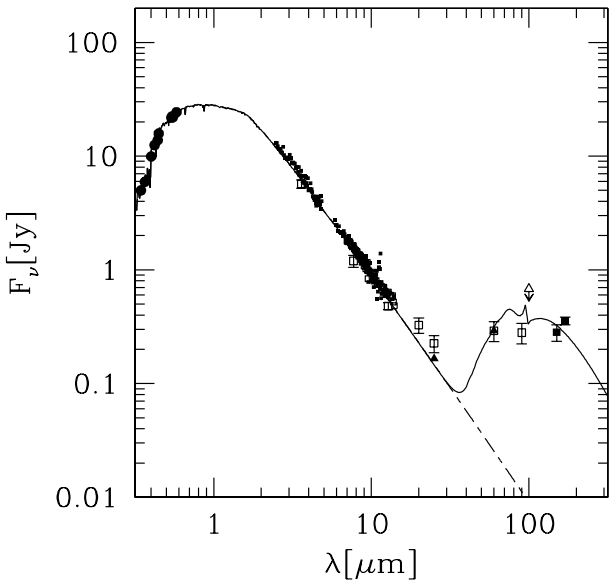

Fig. 4. Overview of the spectral energy distribution of HD 207129, with all measurements. Big dots indicate magnitude measurements taken from the Geneva photometry catalogue (Burki *et al.* 1998, website). Small squares indicate measurements from PHT–S (filled squares) and CAM–CVF (open squares) spectra. Large squares indicate photometry with ISOPHOT P. Filled triangles are IRAS (IFSC data) and the open triangle is the 100 μm IRAS (IFSC) upper limit . The solid line shows the flux derived from the model using cometary dust grains (case B). The dashed line indicates the purely photospheric flux.

information is available. Even the grain size cannot be accurately determined, since the spatial distribution of the excess emission around the star, and thus the distance between dust grains and their heating source are unknown.

We will discuss two different types of grains: on one hand, interstellar silicate grains with optical properties given by Draine & Lee (1984, hereafter DL84), on the other hand, cometary dust grains (Li & Greenberg 1997, hereafter LG97) which are aggregates of silicate grains with an organic and a water ice mantle. DL84 is used here as a reference dust model because it is extensively used in dust related studies.

For the radial distribution of the dust in the disc, we adopt the power-law derived for the surface density in β Pic, $\sigma(r) \propto r^{-1.7}$ (Artymowicz et al. 1989).

We have used a grain size distribution ranging from small grains (1 μm) up to approximately 200 μm. The lower limit of the grains size is still larger that typical interstellar grains (0.1 μm) since the grains found in Vega-like discs and also in the solar system are typically a few μm. The form of the distribution is valid for grains derived from an equilibrated collisional process (Dohnanyi 1969). In this way we take into account that the grains in discs around old main-sequence stars are probably products from the collisions of larger bodies (see discussion in Backman & Paresce 1993). The upper limit to our size distribution is motivated by the fact that the longest wavelength we have observed is 180 μm. The contribution to the 180 μm emission of grains larger than 100 μm in the DL84 model is negligible. The maximum grain size in the LG97 model is determined by the maximum grain mass, which is assumed to be the same as in the DL84 model.

The free parameters to fit the spectrum are then the overall dust mass in the disc in the considered size range, and the inner and outer boundaries of the disc. Important parameters and results from the model are listed in Table 3 for both types of grains. The temperature of the dust grains is found to be very low, thus making an ice coating likely. We also note that these results are in agreement with those of the simpler model used in Sect. 4.

Both versions of the disc model can fit the observed spectral energy distribution equally well. The only main observable discrepancy lies in the region between 25 and 40 μm (see Figure 5), where we do not have additional observations. In both cases we use approximately the same amount of dust, $5 \ldots 6 \times 10^{-8} M_\odot = 1.6 \ldots 1.8 \times 10^{-2} M_\oplus$. However, the silicate dust in case A has to be closer to the star. The cometary dust grains absorb more efficiently, due to their coating with organic material. Therefore, they have to be farther from the star in order to reach the same low temperature as the silicate dust. The temperature near the inner boundary of the disc is 46 K (DL84) and 37 K (LG97). However, the shape of the far-infrared spectrum indicates that the bulk of the emission originates from dust grains at a temperature of about 30 K in both cases. This is much lower than the value of 70 K found for the disc around Vega (e.g. Heinrichsen et al. 1998) or the range of $90 - 140$ K for β Pic (Backman et al. 1992), and this is consistent with the spectral type of the stars.

Table 3. Properties of the disc model

	case A	case B
Grain Material	DL84	LG97
Minimum grain mass	1.1×10^{-11} g	1.1×10^{-11} g
Minimum grain size	1 μm	2.4 μm
Maximum grain mass	9×10^{-6}g	9×10^{-6}g
Maximum grain size	93 μm	227 μm
Size distribution	$f(m) \propto m^{-1.83}$	$f(m) \propto m^{-1.83}$
Surface density	$\sigma(r) \propto r^{-1.7}$	$\sigma(r) \propto r^{-1.7}$
Total mass	$5 \times 10^{-8} M_\odot$	$5.7 \times 10^{-8} M_\odot$
Inner disc radius	200 AU	400 AU
Outer disc radius	500 AU	1000 AU
Max $T_{\rm dust}$	46 K	37 K
Min $T_{\rm dust}$	12 K	17 K
$L_{\rm IR}/L_\star$	1.1×10^{-4}	1.02×10^{-4}

Notes to Table 3: Assumptions are listed above the middle horizontal line and model resulting parameters are listed underneath.

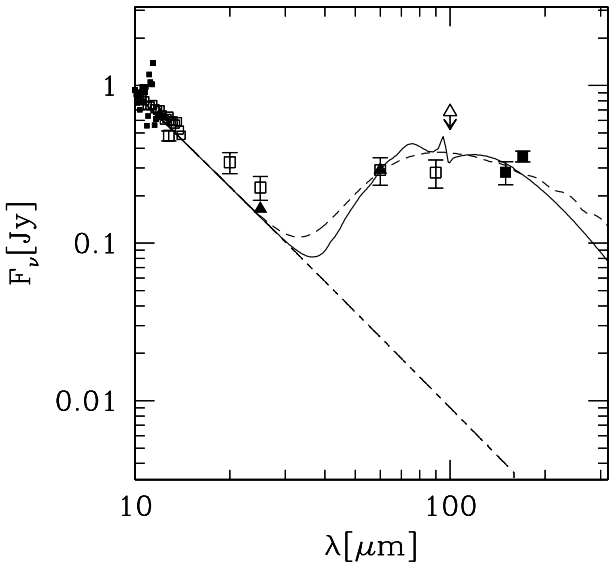

Fig. 5. Comparison between the two different dust compositions. The dashed line indicates case A, the solid line case B. The two cases differ most around 30–40 μm, but they both fit the remaining far–IR excess equally well.

In the following, we concentrate on Case B because we think it provides the most realistic dust model for our purpose. Firstly, in view of the similarity with our solar system, the large distance of the disc from the star suggests that the dust originates from comets rather than from asteroids. Secondly, measurements of interplanetary dust particles with probable cometary origin show that these grains are fluffy aggregates rather than compact silicates grains.

Our prediction of the brightness distribution of model B at a wavelength of 15 μm is given in Figure 6, the wavelength at which we obtained a map with the CAM instrument.

The map in Figure 6 was obtained using a standard scattering phase function of Henyey and Greenstein (Henyey & Greenstein 1941) in which the scattering parameters have been

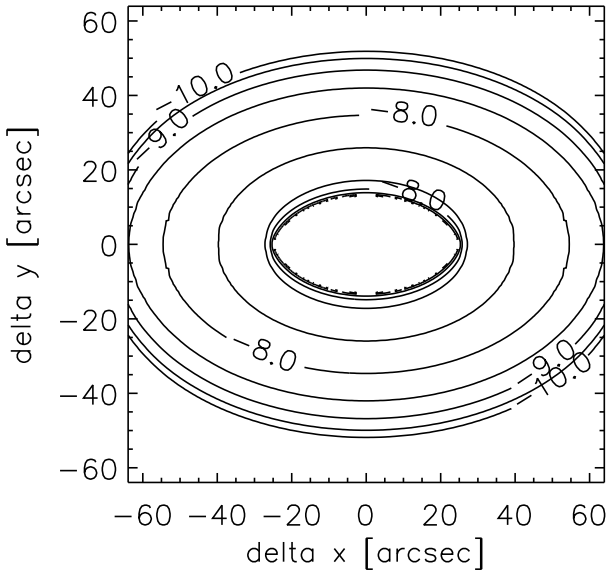

Fig. 6. Theoretical map of case B model at 15 μm, viewed at an angle of 40°. The axes show the distance from the star in arcsec. The isophotes in the figure show $\log F_\nu$ in units Jy/arcsec^2.

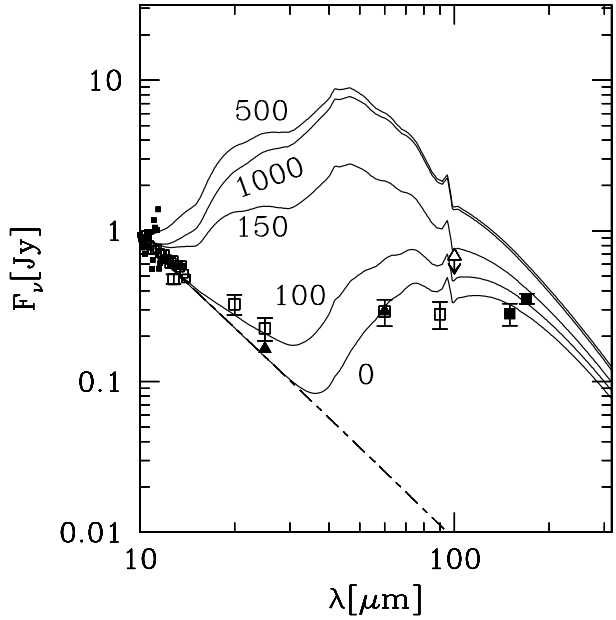

Fig. 7. Evolution timescale of the infrared excess due to radiation forces. The labels on the curves indicate the age of the disc in Myr, starting from the state we observe today.

calculated from the Mie theory. For 2.5 μm grains in model B and at a wavelength of 15 μm, we have the factor of asymmetry $g = 0.18$. Because we do not know the inclination of this disc with respect to the line of sight we took an average angle of 40°.The change of the maximum brightness when the disc is viewed edge-on is for the adopted disc opening angle of 20 degrees only a factor of 4. The map contains both scattered and emitted light from the disc; however, at these wavelengths, the scattered stellar radiation is still dominant. Likewise, the images of the β Pic disc at visual or near infrared wavelengths are also dominated by scattered light. However, HD 207129 is much weaker which makes it impossible to detect the model disc with ISOCAM: The brightest part of the disc, about 20 arcsec away from the star, has a surface brightness of 0.1 μJy/arcsec^2, 2 orders of magnitude below the detection limit of ISOCAM for the circumstances of this measurements.

An important aspect of the HD 207129 disc is that we need a large inner hole to fit the lack of excess emission at 12 and 25 μm. A similar hole has been suggested for the Vega disc, and has been confirmed by recent measurements at 850 μm with JCMT/SCUBA (Holland et al. 1998). In order to investigate the stability of the hole, we have adopted the numerical code developed by Dominik & Habing (1999) and used the dust distribution of case B as the initial condition. In the present calculations, we only consider radiative forces that either expel dust grains from the system or pull them into the star by Poynting–Robertson drag (Burns et al. 1979). On a time scale as short as 50 Myr, a strong infrared excess develops (see Figure 7). A maximum excess at 40 μm is reached after 500 Myr. Then, as the outer disc becomes depleted of small dust grains and more dust has fallen onto the star, the excess slowly decreases. After one stellar lifetime (10 Gyr), an appreciable near-infrared excess still remains.

We conclude that the hole must be filled in about 10^{-3} of the stellar age, unless some agent sweeps it clean. Although the sweeping mechanism is still unclear, the most obvious explanation for this might be the presence of at least one planet (Dominik et al. 1998, and references therein).

6. Conclusion

The G0V star HD 207129 emits approximately 1.1×10^{-4} of its luminosity longward of 25 μm. This excess emission is explained by assuming a disc of dustlike material containing about $10^{-4} M_\oplus$. The dust temperature ranges from 10 to 50 K, and is colder than the dust around Vega-like stars of earlier type. The spatial distribution of the dust emission around HD 207129 is similar to that around other, hotter, Vega-like stars. The results depend little on the assumed dust composition.

The dust distribution in the disc presents a hole of diameter about 400 AU. Particles spiralling inward because of the Poynting–Robertson effect should fill this hole, unless some unseen agent sweeps it clean. The time needed to fill in the hole is only 10^{-3} of the stellar age, which makes the existence of such an unseen agent very likely. It could be explained by the presence of at least one planet.

Acknowledgements. The ISOPHOT data presented in this paper was reduced using PIA, which is a joint development by the ESA Astrophysics Division and the ISOPHOT consortium. In particular, we would like to thank Carlos Gabriel for his excellent support on PIA. The ISOCAM data presented in this paper was analysed using "CIA",

a joint development by the ESA Astrophysics Division and the ISOCAM Consortium. The ISOCAM Consortium is led by the ISOCAM PI, C. Cesarsky, Direction des Sciences de la Matière, C.E.A., France. This research has made use of the Simbad database, operated at CDS, Strasbourg, France, and of NASA's Astrophysics Data System Abstract Service. CD was supported by the "Stichting Astronomisch Onderzoek in Nederland", Astron project 781-76-015.

References

Abergel A., Bernard J.P., Boulanger F., et al.: 1996, *A&A* 315
Artymowicz P., Burrows C., Paresce F.: 1989, *ApJ* 337, 494
Aumann H.H., Gillett F.C., Beichman C.A., et al.: 1984, *Ap.J.* 278, L23
Backman D.E., Gillett F.C., Witteborn F.C.: 1992, *ApJ* 385, 670
Backman D.E., Paresce F.: 1993, In: Levy E.H., Lunine J.I. (eds.), *Protostars and Planets III*, University of Arizona, Tucson
Burns J.A., Lamy P.L., Soter S.: 1979, *Icarus* 40, 1
Cesarsky C.J., Abergel A., Agnèse P., et al.: 1996, *A&A* 315, L32
Dohnanyi J.W.: 1969, *J. Geophys. Res.* 74, 2531
Dominik C., Habing H.J.: 1999, *A&A* in preparation
Dominik C., Laureijs R.J., Jourdain de Muizon M., Habing H.J.: 1998, *A&A* 329, L53
Draine B.T., Lee H.M.: 1984, *ApJ* 285, 89
ESA: 1997, The Hipparcos and Tycho Catalogues. ESA SP–1200
Gabriel C., Acosta-Pulido J., Heinrichsen I., Morris H., Tai W.M.: 1997b, *Astronomical Data Analysis Software and Systems VI* 6, 108
Gabriel C., Acosta-Pulido J., Kinkel U.: 1997a, *Astronomical Data Analysis Software and Systems VI* 6, 112
Gliese W.: 1969, catalogue of nearby Stars. Verlag G. Braun, Karlsruhe
Habing H.J., Bouchet P., Dominik C., et al.: 1996, *A&A* 315, L233
Habing H.J., Dominik C., Jourdain de Muizon M., et al.: 1999, *A&A* in preparation
Heinrichsen I., Walker H.J., Klaas U.: 1998, *MNRAS* 293, L78
Henry T.J., Soderblom D.R., Donahue R.A., Baliunas S.L.: 1996, *AJ* 111, 439
Henyey L.C., Greenstein J.L.: 1941, *Ap.J.* 93, 70
Hildebrand R.H.: 1983, *Q. Jl. R. astr. Soc.* 24, 267
Holland W.S., Greaves J.S., Zuckerman B., et al.: 1998, *Nature* 392, 788
Jayawardhana R., Fisher S., Hartmann L., et al.: 1998, *ApJ* 503, L79
Kessler M.F., Steinz J.A., Anderegg M.E., et al.: 1996, *A&A* 315, L27
Kurucz R.L.: 1993, *ATLAS9 Stellar Atmosphere Programs and 2km/s grid, (Kurucz CD-Rom No. 13)*
Lachaume R., Dominik C., Lanz T., Habing H.: 1999, *A&A* submitted
Laureijs R., Klaas U., Richards P., Schulz B.: 1998, *"ISOPHOT Data User Manual Version 4.0", http://www.iso.vilspa.es/manuals/pht_idum4/*
Lemke D., Klaas U., Abolins J., et al.: 1996, *A&A* 315, L64
Li A., Greenberg J.M.: 1997, *A&A* 331, 291
Malfait K., Bogaert E., Waelkens C.: 1998, *A&A* 331, 211
Mannings V., Sargent A.: 1997, *ApJ* 490, 792
Mayor M., Queloz D.: 1995, *Nature* 378, 355
Moshir M.: 1989, IRAS Faint Source Survey, Explanatory supplement version 1 and tape. Pasadena: Infrared Processing and Analysis Center, California Institute of Technology
Ott S., Abergel A., Altieri B., et al.: 1997, In: Hunt G., Payne H. (eds.), *ASP Conf. Series Vol. 125*, p. 34, ADASS VI
Pasquini L.: 1992, *A&A* 266, 347
Perryman M., Lindegren J., Kovalevsky J., et al.: 1997, *A&A* 323, L49
Plets H., Vynckier C.: 1999, *A&A* 343, 496
Plets H., Waelkens C., Oudmaijer R.D., Waters L.B.F.M.: 1997, *A&A* 323, 513
Rufener F., Nicolet B.: 1988, *A&A* 206, 357
Sargent A.I., Beckwith S.: 1987, *ApJ* 323, 294
Schulz B., Huth S., Kinkel U., et al.: 1999, In: Cox P., Kessler M. (eds.), *The Universe seen by ISO*, ESA – SP 427, in print
Siebenmorgen R., Starck J., Césarsky D., Guest S., Sauvage M.: 1998, *"ISOCAM Data Users Manual Version 4.0", http://www.iso.vilspa.es/manuals/cam_idum4/idum_v4*
Smith B.A., Terrile R.J.: 1984, *Science* 226, 1421
Stecklum B., Käufl H.U., Henning T., et al.: 1998, *ESO Press Release 08/98*
Sylvester R.J., Skinner C.J., Barlow M.J.: 1997, *MNRAS* 289, 831
Walker H.J., Wolstencroft R.D.: 1988, *PASP* 100, 1509
Weissman P.: 1995, *ARA&A* 33, 327